ISSN 0001-4338, Izvestiya, Atmospheric and Oceanic Physics, 2009, Vol. 45, No. 3, pp. 380–391. © Pleiades Publishing, Ltd., 2009.
Original Russian Text © V.A. Dulov, M.V. Kosnik, 2009, published in Izvestiya AN. Fizika Atmosfery i Okeana, 2009, Vol. 45, No. 3, pp. 408–419.

Effects of Three-Wave Interactions in the Gravity–Capillary Range of Wind Waves

V. A. Dulov and M. V. Kosnik

Marine Hydrophysical Institute, National Academy of Sciences of Ukraine, Kapitanskaya ul. 4, Sevastopol, 99011 Ukraine
e-mail: dulov1952@list.ru

Received April 23, 2008; in final form, November 17, 2008

Abstract—The formation of the spectrum of short wind waves from the gravity–capillary and capillary ranges under the effect of three-wave interactions is considered. In order to determine the spectrum, the kinetic equation for wave packets is integrated to the point where the solution is established. Three-wave interactions are described by a collision integral without introducing any additional assumptions simplifying the problem. This calculation procedure reproduces the Zakharov–Filonenko theoretical spectra, which correspond to the cases of energy equipartition and the inertial range. It is shown that the main role of three-wave interactions lies in the energy transfer from the range of short gravity waves to waves with shorter wavelengths. This transfer is accomplished both locally in the Fourier space and as a result of interactions between short and long waves. Its characteristic features are the formation of a dip on the curvature spectrum in the region of a minimum phase velocity of waves and the formation of a secondary peak in the capillary range. The dip is filled and disappears as the wind speed increases. Taking into account the interaction between short and long waves increases the spectrum in the capillary range several times, and the balance between energy input from long waves and viscous dissipation is established in the capillary range. The energy sink caused by three-wave interactions, viscous dissipation, and wind forcing cannot give the stability of the spectrum of short gravity waves.

DOI: 10.1134/S0001433809030116

INTRODUCTION

The modeling of the spectrum of gravity–capillary wind waves with wavelengths lying in the range from centimeters to millimeters has recently been a central problem in the physics of the sea surface [1–6]. By forming water-surface roughness, short wind waves influence the ocean–atmosphere coupling, thus becoming a necessary component of geophysical models. Ocean monitoring from space with the aid of radars with real and synthesized apertures, scatterometers, microwave radiometers, altimeters, and optical facilities is performed owing to electromagnetic scattering and radiation by the sea surface. These phenomena not only depend on the spectrum of gravity–capillary waves but are also frequently determined by it.

Empirical data on the spectrum of short wind waves was gathered from practical radar studies of the sea surface, special-purpose radar experiments [7–9, and others], and investigations of waves in laboratory flumes [10–13]. These data were summarized in empirical models of the spectrum of gravity–capillary waves [2, 3, and others]. We will list the basic conclusions of the cited studies by using the saturation function (curvature spectrum) $B(k, \theta) = k^4F(k, \theta)$ [14], where F is the spectrum of elevations, so $\int k\, F dk d\theta$ is the variance of sea-surface elevations and θ is the angle between the directions of the wind velocity and the wave vector. In the gravity range, the quantity B depends only slightly on k. In the gravity–capillary range, the function $B(k)$ has the following features.

(i) In the entire range of wavelengths, the spectral density increases with the wind speed, and this effect is particularly clearly defined in the range of wavelengths smaller than 20 cm. If the increase is described by the formula $B \sim U^{\alpha}$, where U is the wind speed, then the exponent α, which is ~1 in the gravity range, becomes 3 in the range of wavelengths corresponding to a minimum phase velocity at $\lambda \sim 2$ cm.

(ii) In the case of weak winds, the function $B(k)$ has a distinctive form: a dip is observed in the range of centimeter waves, which is followed by a secondary peak in the range of transition from centimeter to millimeter waves and, further, by an abrupt decrease of the spectral density in the millimeter range. As the wind speed increases, the dip is filled and disappears, whereas the level of the spectrum in the secondary peak increases by an order of magnitude.

(iii) In the range of gravity waves, the angular width of the spectrum increases as the wavelength decreases, whereas the inverse dependence is observed in the range of gravity–capillary waves: the angular width of the spectrum decreases as the wavelength decreases.

Physical modeling of the spectrum of gravity–capillary waves was performed in [1, 4, 5, 15, and others].

This modeling is based on the wave kinetic equation. In a horizontally homogeneous case, this equation is written as

$$\frac{dn(k,\theta)}{dt} = \sum_i Q_i(k,\theta), \tag{1}$$

where $n(\mathbf{k}) = E(\mathbf{k})/\omega(k) = c(k)F(\mathbf{k})$ is the spectral density of wave action, which is related to the spectra of energy and elevations; $\rho F(\mathbf{k})$ is the spectrum of wave energy; ρ is the water density; $\omega(k)$ and $c(k)$ are the eigenfrequency and phase velocity of waves, respectively; and Q_i are the sources that describe wind forcing, viscous dissipation, nonlinear interactions of waves, and other physical ways the spectrum forms. The proposed spectral models differ both in the number of the sources Q_i under consideration and in their specific mathematical descriptions. The desired model of the spectrum is the time-independent solution to Eq. (1), which corresponds to the balance of sources

$$\sum_i Q_i(k,\theta) = 0. \tag{2}$$

In [1, 4], the sources that also model nonlinear interactions are algebraic equations of the spectra, and Eq. (2) is an algebraic equation for $B(k,\theta)$. If nonlinear interactions are included in the number of sources as the integrals of three-wave collisions, then, in order to determine the time-independent solution to Eq. (1), it will be necessary to integrate this equation with respect to time to the point where this solution is established. However, such a problem is rather difficult and laborious for a nonlinear integro-differential equation. Therefore, this problem was previously considered only using approximations whose adequacy could hardly be assessed: waves were assumed to be unidirectional in [15], whereas in [5], additional conditions were imposed on integral characteristics of nonlinear transfer and the problem was reduced to a system of ordinary differential equations.

Although, in due time, each of the models proposed in the cited works yielded a spectrum increasingly approaching observational data, all of these models contain fitting parameters and, sometimes, fitting functions as well. In a number of cases, nonlinear interactions themselves were included in the model in such a way as to cancel the "mismatch" between different mechanisms of forcing and dissipation. Therefore, the role of nonlinear interactions in forming the spectrum of short wind waves is presently unclear.

The local spectrum of short waves is known to vary along the profile of a long wind wave. The action of gravity waves on the mean spectrum in the gravity–capillary range is, to a first approximation, described as a three-wave process [16, 17]. Although the interaction between capillary and gravity waves is a traditional issue in studies of sea-surface dynamics, it seems likely that this problem has not been considered in the context of a statistical description of three-wave interactions.

Energy input from the wind alone is insufficient to maintain the balance of energy for waves of the capillary range [18]. For this reason, the mechanism of capillary-ripple generation by the sharpenings of the short gravity waves that are related to capillary waves by the condition of phase-velocity equality (phase synchronism [19]) was phenomenologically included in the spectral model of [4]. However, three-wave interactions can also transfer energy from short gravity waves to capillary waves. This transfer is most intense if the phase velocity of the long wave is equal to the group velocity of the short wave [17] (group synchronism [17]). However, the role of this cascade transfer in forming the spectrum of capillary waves remains unclear.

The aim of this paper is to study the effects of three-wave interactions on the formation of the spectrum of short wind waves. The three-wave interactions are described by a collision integral without using any additional approximations. The spectrum of short wind waves in the form of a time-independent solution of kinetic equation (1) was calculated by numerically integrating the equation to the point where the solution is established.

THREE-WAVE INTERACTIONS

While energy transfer over the spectrum of gravity waves is accomplished by four-wave interactions (see, for example, [20, 21]), energy transfer in the gravity–capillary range may be performed by three-wave interactions [20, 22]. This result follows the dispersion relation of a general form

$$\omega^2 = gk + Tk^3, \tag{3}$$

where g is the acceleration of gravity and T is the kinematic coefficient of surface tension. The interaction occurs within resonance triads of waves, and it may include both the sum and difference processes:

$$\begin{aligned} \mathbf{k} &= \mathbf{k}_1 + \mathbf{k}_2 \quad \omega = \omega_1 + \omega_2, \\ \mathbf{k} &= \mathbf{k}_1 - \mathbf{k}_2 \quad \omega = \omega_1 - \omega_2. \end{aligned} \tag{4}$$

Here, indices 1 and 2 denote the dependence on the wave vectors $\mathbf{k}_1$ and $\mathbf{k}_2$ and the absence of the index implies a dependence on $\mathbf{k}$. The collision integral that describes the transfer of wave action over the spectrum and presents one of the sources Q_i in kinetic equation (1) has the form

$$\begin{aligned} St(\mathbf{k}) = 4\pi\Big(&\int|V_S|^2(n_1n_2 - n(n_1-n_2)) \\ &\times\delta(\mathbf{k}-\mathbf{k}_1-\mathbf{k}_2)\delta(\omega-\omega_1-\omega_2)d\mathbf{k}_1d\mathbf{k}_2 \\ &+ 2\int|V_D|^2(n_1n_2 - n(n_2-n_1))\delta(\mathbf{k}-\mathbf{k}_1+\mathbf{k}_2) \\ &\times\delta(\omega-\omega_1+\omega_2)d\mathbf{k}_1d\mathbf{k}_2\Big), \end{aligned} \tag{5}$$

where the first and second terms describe the sum and difference processes, respectively, and the interaction coefficients V_S and V_D taken from [23] and transformed using formulas (4) are written as

$$V_S = 2^{-7/2}(b_a b_b\sqrt{cc_1/c_2} + b_a b_c\sqrt{cc_2/c_1} + b_b b_c\sqrt{c_2 c_1/c}),$$

$$V_D = 2^{-7/2}(b_a b_b\sqrt{cc_1/c_2} + -b_a b_c\sqrt{cc_2/c_1} - b_b b_c\sqrt{c_2 c_1/c}),$$

$$b_a = k - k_1 - k_2,\ b_b = k - k_1 + k_2,\ b_c = k + k_1 - k_2.$$

Three-wave interactions may be both local in the **k**-space, when the interaction of waves with wavelengths of the same order of magnitude occurs, and nonlocal. An elegant physical theory of forming the spectrum of capillary waves was proposed in [22]. This theory suggests that local three-wave interactions are a dominant mechanism for forming the spectrum in the entire capillary range except for its shortest wavelength portion, where viscous dissipation becomes important. In this case, the weakly turbulent Kolmogorov spectrum forms in the capillary range. This spectrum is determined by a constant (over the spectrum) energy flux to the dissipation range and is described correspondingly by the equation $St[n] = 0$. Then, in the approximation of isotropic waviness, the saturation function in the capillary range depends on the wave number as

$$B \sim k^{-3/4}. \tag{6}$$

This form of the spectrum was obtained from numerical calculations [24]. The authors of [22] have also found one more isotropic solution to the equation $St = 0$ in the capillary range ($E(\mathbf{k})$ = const) whose physical meaning is the equipartition of energy over wave numbers as a result of local three-wave interactions in the absence of energy sources and sinks. In this case, the dependence of the saturation function on the wave number is

$$B \sim k^2. \tag{7}$$

In nonlocal interactions, wave components are substantially separated in the **k**-space; for example, a gravity wave interacts resonantly with two capillary waves that have very close wavelengths. In this case, the three-wave interaction describes the first nonzero term of the expansion in terms of slopes when a conservative interaction of long and short waves is considered using the method of perturbation theory [16, 17], whereas resonance conditions (4) assume the form

$$\Omega = \mathbf{K}\frac{d\omega}{d\boldsymbol{k}}, \tag{8}$$

where $\mathbf{K}$ and Ω are the wave vector and frequency of a long (i.e., short gravity) wave, respectively, and $\mathbf{k}$ and ω are the wave vector and frequency of a short (capillary) wave, respectively. For unidirectional waves, condition (8) implies that the group velocity of a short wave equals the phase velocity of a long wave—group synchronism [16, 20]. The wave numbers turn out to be related to each other by the equation $K = 4k_m^2/9k$, where the wave number

$$k_m = \sqrt{g/T}$$

corresponds to a minimum phase velocity.

Both local and nonlocal interactions are described by common relation (5); however, the contribution of nonlocal interactions may be described by a simplified expression in the form of a diffusion operator [27], which is the asymptotic form of (5) when $K/k \longrightarrow 0$:

$$St_{nloc}(\mathbf{k}) = \frac{\partial}{\partial k_j}D_{ji}\frac{\partial n}{\partial k_i},$$
$$D_{ji}(\mathbf{k}, \theta) = \pi\int c(K)(\mathbf{Kk})^2 K_j K_i N(\mathbf{K})\delta\left(\Omega - \frac{d\omega}{d\mathbf{k}}\right)d\mathbf{K}, \tag{9}$$

where N is the spectral density of the wave action of long waves. The ratio of the contributions of local and nonlocal interactions was considered in [17, 25] by calculating St for models of real short-wave spectra. The contribution of local interactions in the capillary range turned out to be substantially smaller than the diffusion of action under the influence of long waves, which is described by (9).

NUMERICAL MODEL

The methods and results of numerical calculations of integral (5), as well as the survey of the related problems, can be found in [15, 17, 24, 25, 27] : (i) integral (5) was calculated using an adaptive method, (ii) the volume of calculations was reduced as a result of taking into account the integrand's symmetric properties, (iii) exact analytic expressions were used for the integration boundaries and for determining resonance triads, and (iv) singularities were eliminated by changing the integration variable in their vicinities.

The spectrum $B(k, \theta)$ was studied in the ranges $k_L < k < 15k_m$, where $k_L = (0.1 - 0.7)k_m$ and $0 \le \theta \le \pi$, under the assumption that the spectrum is symmetric about the wind direction $\theta = 0$. Calculations were carried out on a grid with points equally spaced in the variables $\kappa = \ln(k/k_m)$ and θ. The grid spacings were $\Delta k \sim \Delta\theta \sim 5 \times 10^{-2}$. In order to calculate integral (5), we used a 16-point (4×4) interpolation of the spectrum $c(k)B(\mathbf{k})$ by a polynomial cubic in κ and θ (the Lagrange interpolation). As in calculations of the four-wave transfer in the gravity range of wind waves (see, for example, [21]), our model includes a "diagnostic" range (where the spectrum is specified and remains invariant during calculations) and a "prognostic" range (where the spectrum is to be calculated). In the given case, the diagnostic spectrum is the long-wave spectrum that was specified on the grid's extension into the range $k < k_L$.

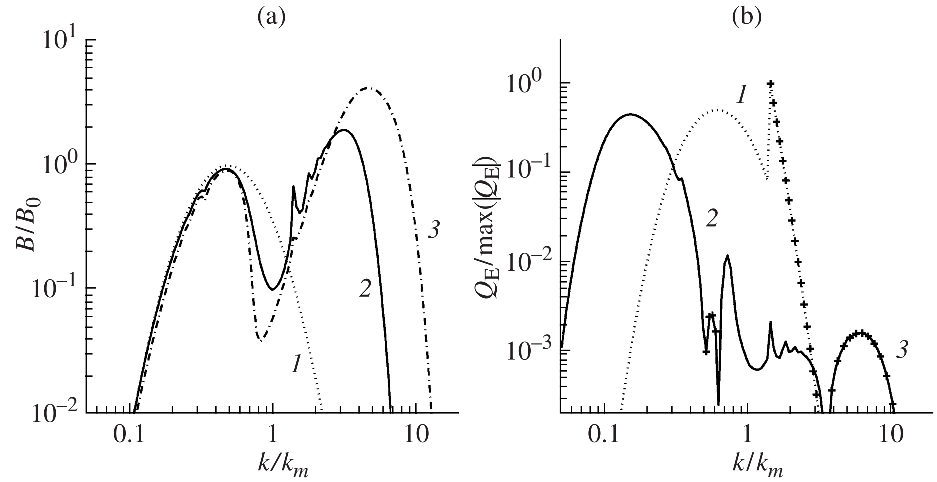

Fig. 1. Evolution of the spectrum localized in the k space: (a) saturation function and (b) spectrum of energy inputs and sinks (the absolute value of Q_E is shown, and the regions where $Q_E > 0$ are indicated by crosses). Curves *1–3* correspond to the moments of time 0, 0.65, and 2.8 s, respectively.

Equation (1) was integrated by a two-step explicit scheme

$$B_j^1 = B_j + \Delta B[B_j]$$

$$B_{j+1} = B_j + (\Delta B[B_j] + \Delta B[B_j^1])/2$$

$$\Delta B[B] = \left(\frac{k^4}{c}\sum_i Q_i[B]\right)\Delta t,$$

where j is the number of iteration. This computation was carried out to the point where the absolute value of the sum of all sources for each grid point was smaller (at least by two orders of magnitude) than the absolute value of each of the sources. The instability of the explicit scheme manifested itself in the fact that the spectrum approached infinity at one of the grid points, then, on further computation, it approached infinity at all of the grid points. This problem, as well as the problem of appearing negative values of the spectral density, was resolved by successively decreasing the integration step Δt.

RESULTS

Local Interactions

First and foremost, let us consider the evolution of the spectrum localized in the k-space in order to reveal the main effects of local three-wave interactions. We specify the initial spectrum as a Gaussian function in κ and θ with a peak at the point $\mathbf{k}_p = (k_p, 0)$:

$$B(k, \theta) = B_0 \exp\left(-\frac{\theta^2}{2\Delta_\theta^2} - \frac{\ln^2(k/k_p)}{2\Delta_\kappa^2}\right). \qquad (10)$$

The kinetic equation may be written as $dn/dt = St[n]$ for all wave components. Let $n_1(t, \mathbf{k})$ be a solution to this equation, so that $n = \alpha n_1(t/\alpha, \mathbf{k})$, $\alpha > 0$) is also a solution. In this sense, the quantity B_0 does not influence the evolution of the spectrum. The normalized spectrum $B(k, \theta)/B_0$ turns out to be the same at an identical number of iterations if the condition $B_0\Delta t = \text{const}$ is fulfilled. We will present below the evolution times for $B_0 = 5 \times 10^{-3}$, which is characteristic of the quantity B for moderate winds (see, for example, [4]).

If the initial spectrum corresponds to a quasi-monochromatic wave $\Delta_\kappa \sim \Delta_\theta \sim 0.1$, its evolution represents a very slow diffusion of the initial perturbation in the $\mathbf{k}$-space. This trivial solution reflects the fact that a monochromatic wave has no partners for an effective three-wave interaction.

Figure 1 shows the evolution of a broadband spectrum with the initial parameters $k_p = k_m/2$, $\Delta_\kappa = 0.5$, and $\Delta_\theta = \pi/4$. Here and below, plots for the saturation function $B(k)$ and for the spectrum of energy inputs and sinks

$$Q_E = \omega(k)St(k).$$

are presented. For convenience, these two quantities in Figs. 1–3 are normalized by B_0 and a maximum value of $|Q_E|$ at $t = 0$, respectively. In order to use a logarithmic scale for representing $Q_E(k)$, the plots of $|Q_E|$ are depicted, whereas the ranges of positive values of the source are marked by plus symbols. Figure 1 presents the plots for $\theta = 0$, and the patterns of variation for other wave directions remain similar. The time intervals from the beginning of evolution for which curves *2* and *3* are constructed correspond to 8.8 and 38 periods of waves with a minimum phase velocity.

The basic feature of this process is energy transfer to the short-wavelength range. When the peak of the initial spectrum is located in the capillary range, energy transfer to the long-wavelength range occurs

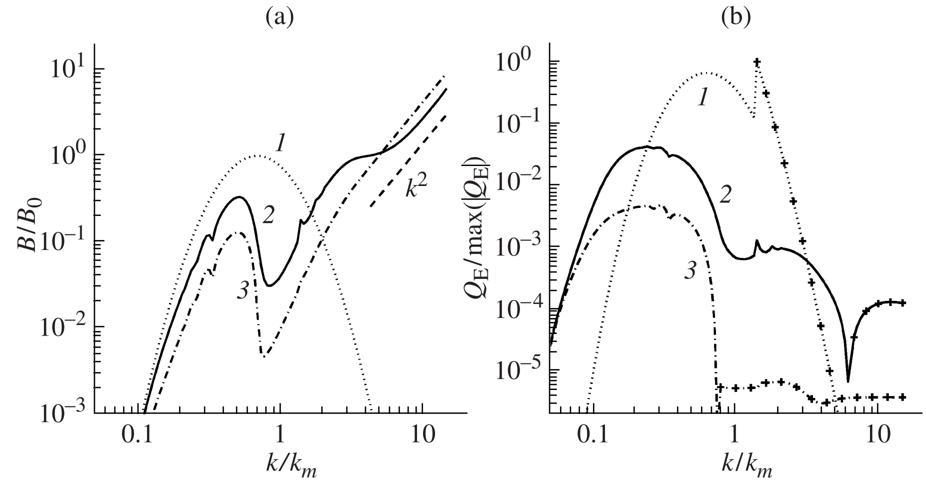

Fig. 2. Establishment of energy equipartition for the isotropic spectrum: (a) saturation function and (b) spectrum of energy inputs and sinks (the regions of energy input, where $Q_E > 0$, are indicated by crosses). Curves *1–3* correspond to the moments of time 0, 4.1, and 33 s, respectively.

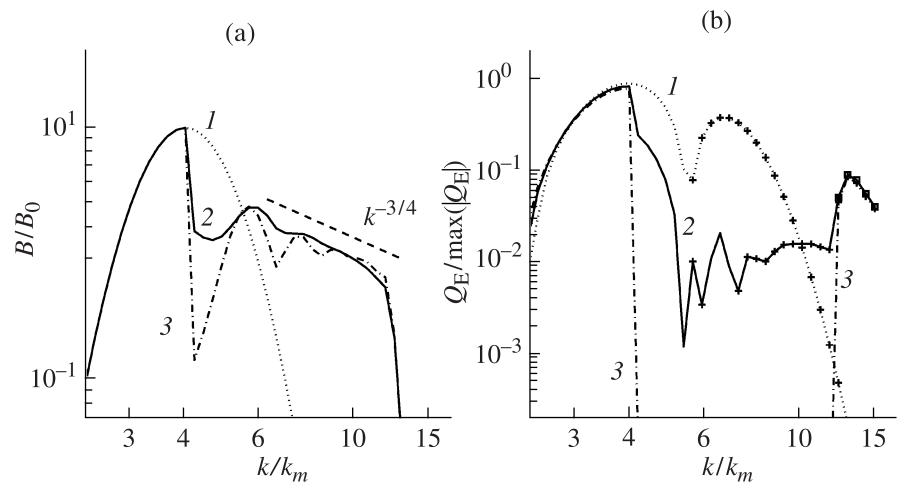

Fig. 3. Formation of the inertial range of the isotropic spectrum in the capillary region: (a) saturation function and (b) spectrum of energy inputs and sinks (the regions of energy input, where $Q_E > 0$, are indicated by crosses, and the dissipation region is indicated by squares). Curves *1–3* correspond to the moments of time 0, 2.25, and 18.6 s, respectively.

as well. However, the latter process is substantially weaker than the dominant energy transfer to short waves.

If energy is originally localized in the range of short gravity and gravity–capillary waves $k_p = O(k_m)$, a dip appears in the vicinity of wave numbers $k \sim k_m$ as a result of energy transfer (see Fig. 1a). In this case, the spectrum in the capillary range may increase by orders of magnitude, which results in the formation of a secondary peak. For different values of k_p, the dip always occurs in the same region, whereas the position of the secondary peak may vary in the course of evolution. Such a character of the solutions appears to be due to the specific form of the source Q_E (see [25–27]); the source is negative in the region $k < \sqrt{2k_m}$ and it undergoes a jump at the point $k = \sqrt{2k_m}$, assuming a maximum positive value. The source has this form at the beginning of evolution (see Fig. 1b, curve *1*). In the course of evolution, the source transforms substantially and its value in the capillary range approaches zero (see Fig. 1b).

In Fig. 1a, a portion of curve *2* has a specific sawtooth form. As is shown in [15], three-wave interactions of unidirectional waves generate energy-transfer cascades that are immiscible in the wave space. In numerical calculations of the evolution of the spectrum of unidirectional waves under the effect of three-wave interactions, these cascades can manifest them-

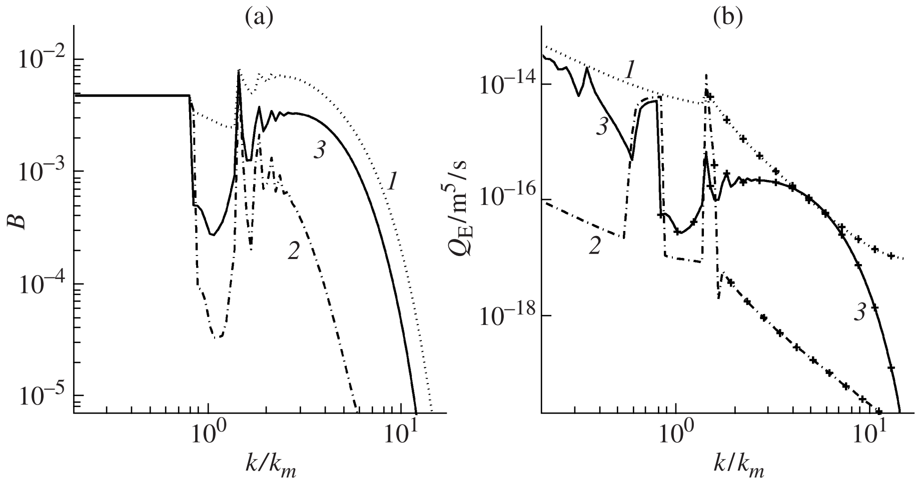

Fig. 4. Establishment of the spectrum of gravity–capillary and capillary waves due to the three-wave energy transfer from the region of short gravity waves: (a) saturation function and (b) spectrum of energy inputs and sinks. Curves *1* and *2* correspond to calculations with different initial conditions (see text) for the moments of time (a) 0.07 and (b) 0.0 s. In the course of evolution, these curves coalesce into curve *3* at 1.3 s.

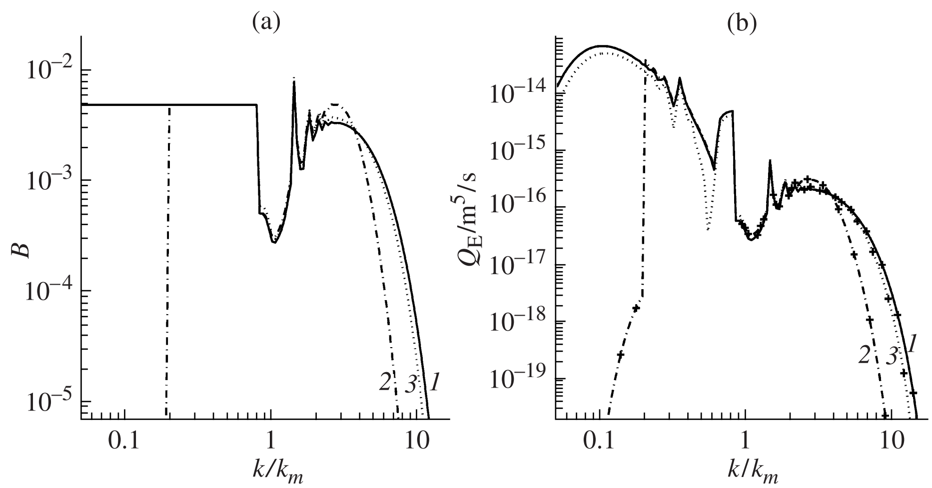

Fig. 5. Steady-state spectra of (a) the saturation function and (b) energy inputs and sinks: (*1*) calculation for isotropic wind waves, (*2*) calculation for isotropic wind waves without considering nonlocal interactions, and (*3*) calculation for anisotropic wind waves (the sections of the spectra are shown at $\theta = 0$ rad).

selves in the spectrum with a saw-tooth form. Such a saw-tooth spectral form sometimes also appears in our calculations for waves with a wide angular spectrum, and the positions of local peaks correspond to calculations for unidirectional waves (cf. Fig. 7 from [15]). As is seen from Fig. 1, a saw-tooth form appeared at the beginning of the evolution (curve *2*); further, however, this form was smoothed in the curvature spectrum (curve *3*) and remained in the spectrum of the source Q_E alone. Below, however, we will present examples in which a saw-tooth form holds in a steady-state spectrum of waves.

Jump variations in $St(k)$ (a jump in St at $k = \sqrt{2k_m}$, Van Gastel's saw) is a formal consequence of using the delta functions of frequencies in collision integral (5). For a more realistic description of wave interactions, these functions should be replaced by their smeared analogues, which reflect the smearing of frequency resonance (4) under the effect of different physical factors (see, for example, [17], where a modification of (5) is obtained with allowance for viscosity). In numerical calculations [28], the saw disappears when wave evolution is considered on a variable current, which actually violates the exact frequency resonance because of the Doppler shifts. The jump of St at $k = \sqrt{2k_m}$ is smoothed if the modulations of the effective acceleration of gravity that are due to orbital motions in long gravity waves are taken into account

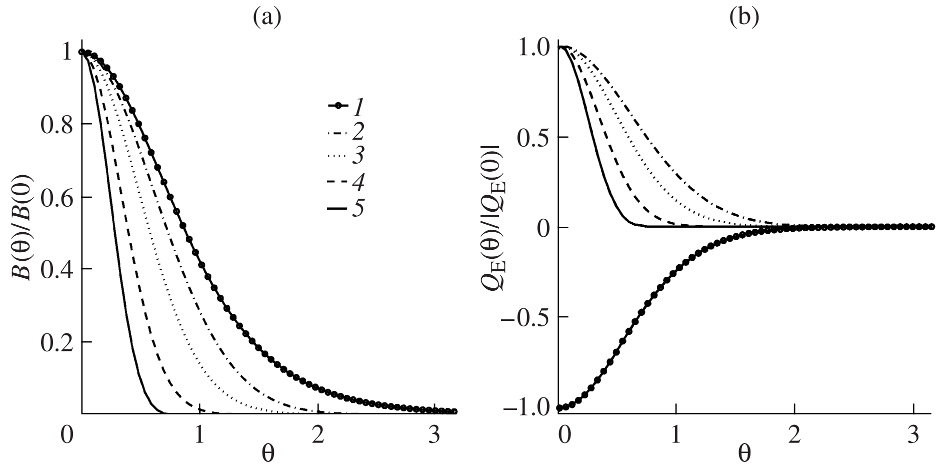

Fig. 6. Angular spectra of (a) the saturation function and (b) energy inputs and sinks for k/k_m values of (*1*) 0.7, (*2*) 1, (*3*) 3, (*4*) 7, and (*5*) 12.

[25]. Thus, jumps and inflections in $St(k)$ are actually absent in more realistic (and, correspondingly, more laborious) calculations. In the given study, however, the appearance of a saw, which hinders the interpretation of results, is due to the accepted simplifications, i.e., to the calculation of St by formula (5) with the use of the delta functions of frequencies.

Figure 2 presents an example of calculation results for an isotropic spectrum. The initial spectrum is given by formula (10) with the parameters $\Delta_\theta = \infty$, $k_p = 0.7k_m$, and $\Delta_\kappa = 0.5$. The behavior of the evolution in this case is the same as in the case of an anisotropic spectrum with a wide angular distribution; energy transfer to the short-wavelength region is a dominant process which generates a dip in the spectrum at $k \sim k_m$ (cf. Fig. 1). However, the calculation covers a rather long time interval: curves *2* and *3* correspond to 58 and 448 periods of waves with a minimum phase velocity. In this case, according to [22], evolution is bound to proceed toward energy equipartition over wave numbers as a result of local three-wave interactions in the absence of other energy sources and sinks. The calculation does demonstrate the establishment of equipartition in the capillary range. The slope of the saturation function $\sim k^2$, which corresponds to equipartition, is also shown in Fig. 2a by a dashed linear segment. The spectrum in the range where this slope is established evolves slowly; the spectrum increases as a result of a continuing energy transfer from the region of its initial localization. However, as is demonstrated by Fig. 1b, the value of the source $|Q_E|$ in the establishment region is several orders of magnitude smaller than that in the region of the efficient energy sink $k \sim k_m$.

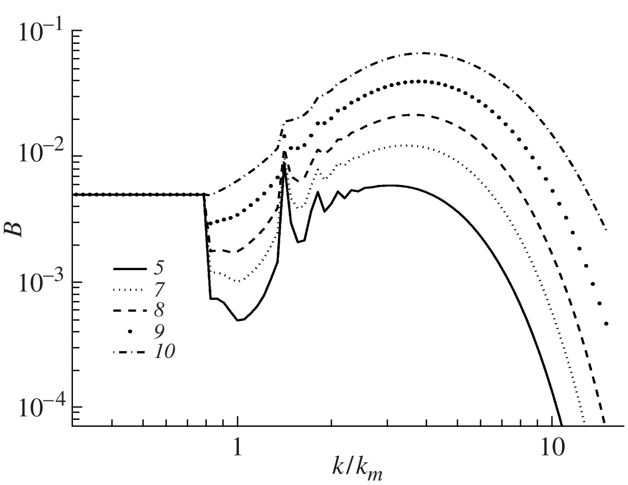

Fig. 7. Filling the dip in the curvature spectrum as the wind speed increases. The figures indicate the wind speed in m/s.

Figure 3 illustrates numerical experiments on the establishment of the Zakharov–Filonenko isotropic flux spectrum in the capillary range. Conditions for the occurrence of the inertial range were ensured as follows. To consider pure capillary waves, the initial spectrum was specified via formula (10) with the parameters $k_p = 4k_m$, and $\Delta\kappa = 0.25$. The spectrum in the region $k < k_p$ was treated as a diagnostic spectrum. The maintenance of a constant spectral level here physically implies the delivery of the necessary energy, i.e., pumping in the long-wavelength region. To provide dissipation in the short-wavelength region $k > 12k_m$, the term γB was added to the right-hand side of Eq. (1), where γ is a smooth monotonic function of k so that $\gamma(12k_m) = 0$ and $\gamma(15k_m) = -4\nu k^2$, $\nu = 1.3 \times 10^{-6}$ m^2/s is the kinematic molecular viscosity of water. In the beginning of the calculation, the balance $St \approx \gamma B$ is established in the dissipation range $k > 12k_m$, so the relation $|St - \gamma B|/St = O(0.01)$ remains valid during further evolution.

The condition $St = 0$ must be satisfied in the inertial range. Curves *2* in Fig. 3 are calculated for 30 periods of waves with a minimum phase velocity and show how the inertial regime is approached in the range $(7–10)k_m$, where the value of $|Q_E|$ becomes several times smaller than in other regions (see Fig. 3b). The slope of the spectrum $B(k)$ in the vicinity of $k \sim 8k_m$ is close to –3/4, which follows from the results of [22]. The dependence $\sim k^{-3/4}$ is also shown in Fig. 3a by a dashed linear segment. However, as the calculation continues, Van Gastel's saw appears in this spectral range. Curve *3* in Fig. 3b, which corresponds to a calculation time of 250 periods of waves with a minimum phase velocity, shows that, physically, the inertial range occurred in the region $(5–12)k_m$, with $|Q_E|$ values that are two to three orders of magnitude smaller than beyond this region. At the same time, only the saw peaks in the spectrum of the saturation function satisfy the law $\sim k^{-3/4}$ (curve *3* in Fig. 3a).

The presented results show the potentials of the calculation method used above and reveal the main function of local three-wave interactions in forming the spectrum of short wind waves (the energy transfer to the short-wavelength region). Curves *2* in the figures demonstrate that major changes in the spectrum that are due to three-wave interactions occur in a characteristic time of 10 to 30 periods of waves with a minimum phase velocity. In [3, 4], it is suggested that three-wave interactions are responsible for the formation of a dip in the curvature spectrum under weak winds. This is strongly supported by the performed calculations; energy transfer due to three-wave interactions occurs so that a dip forms in the region $k \sim k_m$, while a secondary spectral peak forms in the vicinity of $(2–5)k_m$.

Effect of Short Gravity Waves on the Gravity–Capillary Spectrum

Further, we will treat the short-wavelength portion of the spectrum of gravity waves $k < k_L$ as a diagnostic spectrum with a specified quantity $B(k, \theta) = B_0(\theta)$ and calculate the gravity–capillary spectrum in the region $k > k_L$. To isolate the effect of three-wave interactions, we will assume that there are no other energy inputs in the prognostic region of gravity–capillary and capillary waves. For the solution to be established in the prognostic region, we will add the viscous dissipation $Q_{vis} = -4\nu k^2 n$ to the right-hand side of kinetic equation (1) (see, for example, [20]). Then, the wave spectrum in this region will form only due to energy transfer from gravity waves.

However, there are two possibilities for this transfer. In the case of three-wave interactions, waves from the region $k < k_m/\sqrt{2}$ can interact only with shorter waves from the region $k > k_m/\sqrt{2}$ [15, 25]. Therefore, energy is transferred immediately from the diagnostic to the prognostic region only if $k_L \geq k_m/\sqrt{2}$. However, if $k_L < k_m/\sqrt{2}$, energy is transferred from the diagnostic region to the subrange $k > k_L^a$, where $k_L^a > k_m/2$. Energy can be delivered only from this subrange due to three-wave interactions to the second subrange $k_L < k < k_L^a$ to longer waves. For brevity, these cases will be referred to as a direct and an inverse cascade, respectively, and we will consider the direct cascade first.

First and foremost, it is of interest to find out whether the spectrum with a level B comparable to B_0 can be established in the region $k > k_L$ only at the expense of three-wave transfer of energy from the region of short gravity waves and its viscous dissipation. In other words, whether the mere presence of short gravity waves is sufficient for the existence of the spectrum of gravity–capillary and capillary waves. Our numerical experiments have shown that this is actually possible for the direct cascade. The steady-state spectrum does not depend on the initial conditions in the prognostic region and is controlled by the calculation parameters B_0 and k_L. Figure 4 shows the results of two calculations for an isotropic spectrum with the parameters $B_0 = 5 \times 10^{-3}$ and $k_L = 0.8$, which differ in initial conditions in the prognostic region. Curves *1* and *2* correspond to the initial conditions $B = B_0$ and $B = B_0/500$, respectively, whereas curve *3* shows the calculation result to which both solutions converge in 1.3 s (17 periods of waves with a minimum phase velocity). Figure 4a illustrates the establishment of the spectrum when the function $B(k)$ rapidly assumes a characteristic form (curves *1* and *2* in Fig. 4a correspond to the time 0.07 s). Figure 4b shows the absolute values of energy inputs and sinks because of three-wave interactions: curves *1* and *2* correspond to the initial distributions of Q_E, whereas curve *3* corresponds to the steady-state solution. The evolution of the source Q_E proceeds so that its balance with viscous dissipation is established first ($|St + Q_{\text{vis}}|/St = O(0.01)$) for the shortest capillary waves. After that, variations in B and Q_E in this region occur with balance retention, and the region itself extends because it includes longer waves. The balance holds for all capillary waves $k > 2k_m$ for 0.4 s. As can be seen from comparing curves *1* and *2* with curve *3* (Fig. 4b), the spectral form of the source Q_E changes substantially in the course of adjusting the three-wave energy transfer to the action of viscous attenuation.

While local interactions ensure energy transfer from the region $k \sim k_L$ to the region of a secondary peak, nonlocal interactions accomplish an immediate energy transfer from short gravity waves to capillary waves. To emphasize the effect of nonlocal interactions, we carried out calculations that differed from the previous calculations by the absence of gravity waves with wavelengths longer than 8.5 cm ($B = 0$ if $k < 0.2k_m$). The results are compared in Fig. 5, where curves *1* are calculated with allowance for nonlocal interactions and correspond to the steady-state solution, which is shown by curve *3* in Fig. 4, and curves *2* are calculated without considering nonlocal interactions. The main difference in the form of the spectrum occurs in the region of capillary waves. As is seen in Fig. 5a, due to nonlocal interactions, the spectral level for $k > 5k_m$ increases by an order of magnitude. Figure 5b shows that the decrease of the spectral level results from a strong reduction of energy input to the region of capillary waves in the absence of a three-wave energy sink for short gravity waves from the range $k < 0.2k_m$.

Figure 5 also depicts the sections of the steady-state spectra for $\theta = 0$ (curves *3*) that are calculated for the spectrum with its diagnostic part

$$B(k, \theta) = B_0/\cosh^2\beta\theta, \tag{11}$$

where $\beta = 1$ and B_0 and k_L have the same values as before. As follows from the figure, the spectrum's anisotropy does not lead to new features in the form of spectra in the principal direction.

The sections of the steady-state spectra $B(k, \theta)$ for different values of k/k_m and the related sections of Q_E are shown in Fig. 6. For all directions, the function $B(k)$ exhibits a dip at $k \sim k_m$ and a secondary spectral peak, which is followed by a rapid decrease with increasing k. In the principal direction, the solution is established in less than 2 s, whereas it is established more slowly in lateral directions. (The figure shows the spectra corresponding to 5.6 s. The angular width of the spectra decreases monotonically as k increases.)

As was noted in [15, 25], the main contribution to the collision integral is made by the interactions of waves with close directions. In other words, the intensity of three-wave transfer in direction θ, which is determined by the spectral level $B(\theta)$ in the diagnostic region, turns out to be lower than this intensity in the principal direction, which explains the slowdown of the establishment of the spectrum for lateral directions. The reduction of the intensity of three-wave interactions at lateral directions are likely to result in the fact that other energy inputs prove to be dominant at these directions (see, for example, [6]). It should be noted that calculations show a monotonic decrease in the angular width of the spectra with increasing k in the entire range from short gravity to capillary waves. According to experimental data [7, 9, 12], the angular width of the spectrum of short waves does decrease as k increases in the range $k < k_*$, where k_* lies in the gravity–capillary range and corresponds approximately to a secondary peak; however, as k increases further, the angular width increases.

The above main results of calculations are also valid for other values of B_0 in the range from 10^{-5} to 10^{-2} and for other angular dependences of diagnostic spectrum (11) with β values from 0 to 4.

Effect of Wind Forcing

According to experimental data, a dip in the spectrum B disappears when the wind speed increases. Figure 7 shows the calculation results obtained for the region of the direct cascade $k_L \geq k_m/\sqrt{2}$, which reproduce this phenomenon.

It is necessary to note that the level of the spectrum, as well as its dependence on the wind speed, is substantially determined by the models of wind forcing and wave-energy dissipation [1, 4]. In this study we focused on the effect of three-wave interactions on the form of the spectrum, leaving aside the problem of reliably determining the spectral level. Taking into account the qualitative character of our calculations and the uncertainty in specifying the spectral level and the angular distribution in the diagnostic region, we chose the simplest model to construct Fig. 7. The wave spectrum was assumed to be isotropic, and the wind forcing was described by adding the term $Q_{in} = \omega\beta_w n$ to the right-hand side of kinetic equation (2), where the wind–wave interaction coefficient was written as $\beta_w = 0.02\ (u_*/c)^2$ [29] and the friction velocity was estimated by the aerodynamic formula $u_*^2 = C_D U^2$ with the drag coefficient $C_D = 1.5 \times 10^{-3}$. As in Figs. 5 and 6, the parameters of the spectrum in the diagnostic region were taken equal to $k_L = 0.8k_m$ and $B = 5 \times 10^{-3}$. The characteristic time in whichthe solutions are established is 1 s. As is seen in Fig. 7, the dip in the curvature spectrum, which is due to three-wave interactions, is actually filled as the wind speed increases.

Instability of the Inverse Cascade

If $k_L < k_m/\sqrt{2}$ and the wind forcing is absent, the solution $B(\mathbf{k}) = 0$ is established in the prognostic region. Although the balance between energy input and viscous dissipation can be achieved in individual regions $k \sim k_m$ in the course of establishment, the evolution of the spectrum does not cease and its level in the prognostic region decreases further, becoming several orders of magnitude smaller than B_0.

If the wind forcing in the form $Q_{in} = \omega\beta_w n$ (where different formulas proposed in [1, 29, 30] are used) is added to the right-hand side of kinetic equation (1), an instability appears in the form of an unbounded growth of β_w within a certain portion of the region $k_L < k < \sqrt{2k_m}$. These features of the inverse cascade can be explained qualitatively as follows.

Let indices 0, 2, and 1 be assigned to the ranges $k_L < k < k_m/\sqrt{2}$, $k_m/\sqrt{2} < k < \sqrt{2}\,k_m$, and $k > \sqrt{2}\,k_m$, respectively. Only difference processes are possible in intervals 0 and 2, so that $k_0 = k_1 - k_2$ and, according to (2), the combinations of spectra under the integrals for *St* are written as $n_1n_2 - n_0(n_2 - n_1)$. Taking into account that $k_0 < k_2 < k_1$ and that the spectra of action decrease by a law close to the power law with an exponent of –3.5, we retain the term $-n_0n_2$ alone in the combination of spectra. Because the main contribution to the integral *St* is made by the immediate vicinity of the integration boundaries k_0 and k_2, the kinetic equation may be approximately written as

$$\frac{dn_0}{dt} = n_0(b_0 - a_0n_2),\ \frac{dn_2}{dt} = n_2(b_2 - a_2n_0), \qquad (12)$$

where the coefficients a are positive according to (2) and the first terms on the right-hand sides are the differences between the wind forcing and the viscous dissipation; i.e., $b = \omega b_{in} - 4\nu k^2$. If the wind forcing is absent ($b < 0$), system (12) has the stationary solution $n_0 = n_2 = 0$. If the two coefficients b are positive due to the wind forcing, there is the nontrivial stationary solution $n_0 = b_2/a_2$, $n_2 = b_0/a_0$. Consider the small perturbations Δn_0 and Δn_2 in this solution. To within linear terms, the equations for these perturbations may be written as

$$\frac{d\Delta n_0}{dt} = -\left(\frac{b_2a_0}{a_2}\right)\Delta n_2 \quad \frac{d\Delta n_2}{dt} = -\left(\frac{b_0a_2}{a_0}\right)\Delta n_0,$$

where the combinations of coefficients in parentheses are positive. It follows that the stationary solution is unstable against perturbations with different signs. If $\Delta n_0 > 0$ and $\Delta n_2 < 0$, then, in the course of time, Δn_0 increases at an increasing rate, whereas n_2 continues to decrease. If $\Delta n_0 < 0$ and $\Delta n_2 > 0$, n_0 continues to decrease, while Δn_2 increases at an increasing rate. This is the same pattern of irregular instability development in the solution as was observed in our numerical calculations when the saturation function increased without bound either in interval 0 or interval 2.

Thus, the physical mechanisms considered above—three-wave energy transfer, viscous dissipation, and wind forcing—do not ensure the existence of the wave spectrum in the region $k < k_m/\sqrt{2}$; i.e., they do not lead to a steady-state solution of the kinetic equation. In order to construct a model for a real spectrum, it is necessary to take into account other mechanisms, for example, the dissipation of gravity waves through the generation of capillary ripples under microbreakings [5].

CONCLUSIONS

The effects of three-wave interactions on the formation of the spectrum of short wind waves were studied. The spectrum was calculated by integrating the kinetic equation with respect to time to the point where a steady-state solution was established. The collision integral was taken in its original form without using any additional approximations, which made the calculations easier. The averaged effect of short gravity waves on capillary waves was automatically included in the calculation results. A numerical implementation of the calculations made it possible to reproduce the spectra for the cases of energy equipartition and a constant energy flux in the inertial range, which were proposed for the capillary region in [22]. The following conclusions were made on the basis of the results obtained in this study.

(1) Three-wave interactions are an especially effective mechanism of energy transfer from the region of short gravity waves to the regions of capillary and gravity–capillary waves. If the energy dissipation of capillary and gravity–capillary waves is determined by viscosity alone ($Q_{vis} = -4\nu k^2 n$), the presence of short gravity waves alone is sufficient for waves whose spectral density is in agreement with observations in the order of magnitude to exist in these regions. In this case, the spectrum of capillary and gravity –capillary waves is established due to three-wave interactions in no longer than 1.5 s. The spectrum in the capillary region is the result of the balance between the direct energy input from short gravity waves (the averaged result of interaction between short and long waves, i.e., three-wave interactions that are nonlocal in the *k*-space) and viscous losses.

(2) Due to three-wave interactions in the gravity–capillary region, the experimentally observed typical form of the curvature spectrum is established: there is a dip in the region $k \sim k_m$ (i.e., for wavelengths of about 2 cm) followed by a secondary spectral peak. With allowance for a wind forcing, in accordance with observations, the dip is filled and disappears as the wind speed increases. It is possible that this effect explains the fact that the spectral density of precisely two-centimeter waves depends most strongly on the wind speed ($\sim U^3$).

(3) The three-wave energy transfer combined with wind forcing and viscous dissipation cannot ensure the stability of the spectrum of short gravity waves in the region $k < k_m/\sqrt{2}$. To stabilize the spectrum in this region, it is necessary to introduce additional wave-energy losses to the kinetic equation. It seems logical to take into account the dissipation related to microbreakings and the generation of capillary ripples [6].

(4) The angular distribution of wave energy that is established as a result of three-wave interactions in the gravity–capillary and capillary regions is characterized by a monotonic decrease in the angular width of the spectrum with a decreasing wavelength. This result corresponds to empirical notions for the region

of short gravity waves [7–9], but it is inconsistent with experimental data related to the capillary region [12]. While correctly considering three-wave interactions gives a realistic spectrum form at the dominant wave directions, introducing additional sources to the right-hand side of the kinetic equation seems to be expedient at lateral directions, where the energy of waves is smaller and, correspondingly, the intensity of three-wave interactions is small (see, for example, [6]).

What is the role of the above effects in forming the actual spectrum of short wind waves? The answer to this question could be given by the calculations that, along with three-wave interactions, viscous dissipation, and energy input from the wind, take into account the nonlinear dissipation of short gravity waves due to microbreakings, as well as the accompanying generation of spurious capillary ripple [4, 18, 19]. It is necessary to note that, according to this study, allowing for nonlinear dissipation is of fundamental importance for the stability of the spectrum of short gravity waves. However, no spurious capillary ripple is generated in the immediate vicinity of k_m, although dissipation becomes unimportant as the spectral level is decreased because of the nonlinear character of dissipation. Therefore, it is expected that the effect of dip formation in the curvature spectrum in the vicinity of k_m will also persist if these two sources are taken into account.

ACKNOWLEDGMENTS

The authors are grateful to V.N. Kudryavtsev for fruitful discussions. This study was supported by INTAS (grant no. 05-1000008-8014), INTAS/ESA (grant no. 06-1000025-9264, DEMOSS), and the Project MONRUK of the FP-6.

REFERENCES

1. M. A. Donelan and W. J. Pierson, "Radar Scattering and Equilibrium Ranges in Wind-Generated Waves with Application to Scatterometry," J. Geophys. Res. C **92**, 4971–5029 (1987).
2. R. J. Apel, "An Improved Model of the Ocean Surface Wave Vector Spectrum and Its Effects on Radar Backscatter," J. Geophys. Res. **99**, 16 269–16 290 (1994).
3. T. Elfouhaily, B. Chabron, K. Katsaros, et al., "A Unified Directional Spectrum for Long and Short Wind-Driven Waves," J. Geophys. Res. C **102**, 15 781–15 796 (1997).
4. V. N. Kudryavtsev, V. K. Makin, and B. Chapron, "Coupled Sea Surface–Atmosphere Model: Part 2. Spectrum of Short Wind Waves," J. Geophys. Res. C **104**, 7625–7639 (1999).
5. G. Caudal, "A Physical Model for the Narrowing of the Directional Sea Wave Spectra in the Short Gravity to Gravity–Capillary Range," J. Geophys. Res. C **107**, 12.1–12.9 (2002).
6. V. Kudryavtsev and J. Johannessen, "On Effect of Wave-breaking on Short Wind Waves," Geophys. Rev. Lett. **31**, doi: 10.1029/2004GL020619, L20310 (2004).
7. A. K. Fung and K. K. Lee, "A Semi-Empirical Sea-Spectrum Model for Scattering Coefficient Estimation," IEEE J. Ocean. Eng. **OE–7** (4), 166–176 (1982).
8. H. Masuko, K. Okamoto, M. Shimada, et al., "Measurement of Microwave Backscattering of the Ocean Surface Using X Band and Ka Band Airborne Scatterometers," J. Geophys. Res. C **91**, 13 065–13 083 (1986).
9. G. Caudal and D. Hauser, "Directional Spreading Function of the Sea Wave Spectrum at Short Scale, Inferred from Multifrequency Radar Observations," J. Geophys. Res. C **101**, 16 603–16 613 (1996).
10. B. Jahne and K. S. Riemer, "Two-Dimensional Wave Number Spectra of Smallscale Water Surface Waves," J. Geophys. Res. **95**, 11 531–11 546 (1990).
11. P. A. Hwang, D. B. Trizna, and Wu. Jin, "Spatial Measurements if Short Wind Waves Using a Scanning Slope Sensor," Dyn. Atmos. Oceans **20**, 1–23 (1993).
12. X. Zhang, "Wavenumber Spectrum of Very Short Wind Waves: An Application of 2-D Slepian Windows to the Spectral Estimation," J. Atmos. Ocean. Tech., No. 11, 489–505 (1995).
13. T. Hara, E. J. Bock, and M. Donelan, "Frequency-Wavenumber Spectrum of Wind-Generated Gravity–Capillary Waves," J. Geophys. Res. **102**, 1067–1072 (1997).
14. O. M. Phillips, "Spectral and Statistical Properties of the Equilibrium Range in Wind-Generated Gravity Waves," J. Fluid Mech. **156**, 505–531 (1985).
15. K. Van Gastel, "Nonlinear Interactions of Gravity–Capillary Waves: Lagrangian Theory and Effects on the Spectrum," J. Fluid Mech. **182**, 449–523 (1987).
16. M. Stiassnie, "On the Equilibrium Spectrum of Gravity–Capillary Waves," J. Phys. Oceanogr. **26** (6), 1093–1098 (1996).
17. V. A. Dulov, "Nonconservative Weakly Nonlinear Interaction between Gravity and Capillary Waves," Izv. Akad. Nauk, Fiz. Atmos. Okeana **38**, 398–401 (2002) [Izv., Atmos. Ocean. Phys. **38**, 354–357 (2002)].
18. V. N. Kudryavtsev, "Semiempirical Model of the Spectrum of Capillary Ripple," Morsk. Gidrofiz. Zh., No. 2, 3–14 (1996).
19. S. A. Ermakov, K. D. Ruvinskii, S. G. Salashin, et al., "Experimental Study of the Generation of Gravity–Capillary Ripple by Strongly Nonlinear Waves on the Surface of a Deep Liquid," Izv. Akad. Nauk SSSR, Fiz. Atmos. Okeana **22**, 835–842 (1986).
20. O. M. Phillips, *The Dynamics of the Upper Ocean* (Cambridge Univ. Press, Cambridge; Gidrometeoizdat, Leningrad, 1980).
21. G. J. Komen, L. Cavaleri, M. Donelan, et al., *Dynamics and Modelling of Ocean Waves* (Cambridge Univ. Press, Cambridge, 1994).
22. V. E. Zakharov and N. N. Filonenko, "Weak Turbulence of Capillary Waves," Prikl. Mekh. Tekh. Fiz., No. 5, 62–67 (1967).
23. V. P. Krasitskii, "On Reduced Equation in the Hamiltonian Theory of Weakly Nonlinear Surface Waves," J. Fluid Mech. **272**, 1–20 (1994).

24. A. N. Pushkarev and V. E. Zakharov, "Turbulence of Capillary Waves," Phys. Rev. Lett. **76**, 3320–3323 (1996).

25. V. A. Dulov, "Weakly Nonlinear Transfer of Energy in the Gravity–Capillary Range of Surface Waves: the Effect of the Spectral Form," Morsk. Gidrofiz. Zh., No. 1, 21–31 (2001).

26. G. R. Valenzuela and M. B. Laing, "Nonlinear Energy Transfer in Gravity–Capillary Wave Spectra," J. Fluid Mech. **54**, 507–520 (1972).

27. V. G. Polnikov, "Nonlinear Three-Wave Interactions in the System of Gravity–Capillary Waves in Water," Izv. Akad. Nauk, Fiz. Atmos. Okeana **41**, 253–266 (2005) [Izv., Atmos. Ocean. Phys. **41**, 228–241 (2005)].

28. K. Van Gastel, "Imaging of X-Band Radar of Sub-Surface Features: A Nonlinear Phenomenon," J. Geophys. Res. C **92**, 11 857–11 865 (1987).

29. W. J. Plant, "A Relationship between Wind Stress and Wave Slope," J. Geophys. Res. C **87**, 1961–1967 (1982).

30. R. W. Stewart, "The Air–Sea Momentum Exchange," Boundary-Layer Meteorol. **6**, 151–167 (1974).